1521-0103/344/1/141–154$25.00
THE JOURNAL OF PHARMACOLOGY AND EXPERIMENTAL THERAPEUTICS

http://dx.doi.org/10.1124/jpet.112.199497
J Pharmacol Exp Ther 344:141–154, January 2013

Evaluation of Metabolically Stabilized Angiotensin IV Analogs as Procognitive/Antidementia Agents[S]

Alene T. McCoy, Caroline C. Benoist, John W. Wright, Leen H. Kawas, Jyote M. Bule-Ghogare, Mingyan Zhu, Suzanne M. Appleyard, Gary A. Wayman, and Joseph W. Harding

Department of Veterinary and Comparative Anatomy, Pharmacology, and Physiology (A.T.M.,C.C.B., J.W.W., L.H.K., J.M.B.-G., M.Z., S.M.A., G.A.W., J.W.H.), Department of Psychology (J.W.W., J.W.H.), and Program in Pharmacology and Toxicology (A.T.M., L.H.K., J.W.H.), Washington State University, Pullman, Washington

Received August 22, 2012; accepted October 9, 2012

ABSTRACT

Angiotensin IV (AngIV: VYIHPF)–related peptides have long been recognized as procognitive agents with potential as antidementia therapeutics. Their development as useful therapeutics, however, has been limited by physiochemical properties that make them susceptible to metabolic degradation and impermeable to gut and blood-brain barriers. A previous study demonstrated that the core structural information required to impart the procognitive activity of the AngIV analog, norleucine^1-angiotensin IV, resides in its three N-terminal amino acids, Nle-Tyr-Ile. The goal of this project was to chemically modify this tripeptide in such a way to enhance its metabolic stability and barrier permeability to produce a drug candidate with potential clinical utility. Initial results demonstrated that several N- and C-terminal modifications lead to dramatically improved stability while maintaining the capability to reverse scopolamine-induced deficits in Morris water maze performance and augment hippocampal synaptogenesis. Subsequent chemical modifications, which were designed to increase hydrophobicity and decrease hydrogen bonding, yielded an orally active, blood-barrier permeant, metabolically stabilized analog, *N*-hexanoic-Tyr-Ile-(6) aminohexanoic amide (dihexa), that exhibits excellent antidementia activity in the scopolamine and aged rat models and marked synaptogenic activity. These data suggest that dihexa may have therapeutic potential as a treatment of disorders, such as Alzheimer's disease, where augmented synaptic connectivity may be beneficial.

Introduction

Multiple studies have documented the ability of angiotensin IV (AngIV) and several AngIV analogs to facilitate long-term potentiation, learning, and memory consolidation (Braszko et al., 1988; Wright et al., 1999; Kramar et al., 2001; Lee et al., 2004); increase cerebral blood flow (Kramar et al., 1997); and provide neuroprotection (Faure et al., 2006). More significantly, the acute application of AngIV or one of its analogs, Nle-Tyr-Ile-His-Pro-Phe (Nle^1-AngIV), reverses deficits in dementia models induced by 1) treatment with the cholinergic muscarinic receptor antagonist scopolamine (Pederson et al., 2001), 2) kainic acid injections into the hippocampus (Stubley-Weatherly et al., 1996), 3) perforant path cuts (Wright et al., 1999), and 4) ischemia resulting from transient four-vessel occlusion (Wright et al., 1996).

These observations have long encouraged the notion that AngIV-based pharmaceuticals may have potential as antidementia therapeutics (Mustafa et al., 2001; von Bohlen und Halbach, 2003; Gard, 2004, 2008; De Bundel et al., 2008; Wright and Harding, 2010). The transformation of AngIV and earlier described analogs into clinically useful agents has been impeded by their lack of metabolic stability and inability to penetrate the blood-brain barrier (BBB). This later limitation of AngIV-related peptides results from considerations of molecular size, overall hydrophobicity, and hydrogen bonding potential as reflected by the size of the encompassing hydration sphere. In an initial attempt to transform the highly active AngIV analog, Nle^1-AngIV, into an effective drug, we evaluated the procognitive activity of a series of

This work was supported in part by the Edward E. and Lucille I. Lainge Endowment for Alzheimer's Research, funds provided for medical and biological research by the State of Washington Initiative Measure No. 171 to J.W.W.; the National Institutes of Health [Grant MH086032]; and a Hope for Depression Research Foundation grant to G.A.W.

J.W.W. and J.W.H. are founders and shareholders of M^3 Biotechnology, LLC, which is developing pharmaceuticals based on this technology.

An abstract of part of this work has appeared at the following meeting: Benoist CC, Wright JW, Zhu M, Kawas LH, Appleyard SA, Wayman GA, and Harding JW (2010) Evaluation of an orally active angiotensin IV analogue (Abstract #856.3). *Society for Neuroscience Meeting;* 2010; San Diego, CA.

A.T.M., C.C.B., and J.W.W. contributed equally to the generation and presentation of the data described in this study.

dx.doi.org/10.1124/jpet.112.199497.

[S] This article has supplemental material available at jpet.aspetjournals.org.

ABBREVIATIONS: ACN, acetonitrile; aCSF, artificial cerebrospinal fluid; AngIV, angiotensin IV; ANOVA, analysis of variance; AUC, area under the curve; BBB, blood-brain barrier; Cl_{int}, average intrinsic clearance; C_{max}, concentration in plasma extrapolated to time zero (C_0); dihexa, *N*-hexanoic-Tyr-Ile-(6) amino-hexanoic amide; DMSO, dimethyl sulfoxide; HGF, hepatocyte growth factor; HPLC, high-pressure liquid chromatography; logP, log transformation of the octanol/water partition ratio and measure of hydrophilicity; mEPSC, miniature excitatory postsynaptic currents; Nle^1-AngIV, Nle-Tyr-Ile-His-Pro-Phe; PBS, phosphate-buffered saline; P_{eff}, predicted effective human jejunal permeability; PIPES, piperazine-*N*,*N*′-bis(2-ethanesulfonic acid); $t_{1/2}$, terminal elimination rate constant; V_d, volume of distribution; VGLUT1, vesicular glutamate transporter 1.

C-terminal truncated peptides derived from Nle[1]-AngIV (Benoist et al., 2011). These initial studies demonstrated that fragments as small as tri- and tetrapeptides retained the desired procognitive/antidementia properties of Nle[1]-AngIV. Furthermore, the study by Benoist et al. (2011) identified a likely explanation for the observed activity, namely, the capacity to augment synaptic connectivity through the induction of new functional synapses. Increased functional connectivity could be inferred from the augmented spinogenesis, the colocalization of synaptic markers on the newly formed dendritic spines, and a concomitant enhancement of miniature excitatory postsynaptic currents.

The practical outcome of the study by Benoist et al. (2011) was that the information required to support Nle[1]-AngIV–dependent procognitive activity resided in the N-terminal tripeptide. This realization suggested that, with proper medicinal chemical modifications, it may be possible to develop clinically useful small-molecule cognitive enhancers derived from Nle[1]-AngIV. Despite the small size of the tri- and tetrapeptides, a property ultimately necessary for BBB permeability, these molecules were metabolically unstable and likely too hydrophilic to breach the BBB. Thus, using these molecules as templates, we set out to increase metabolic stability and hydrophobicity by incorporating various structural changes that were primarily targeted at the N terminus, the primary site of peptidase-dependent degradation (Abhold and Harding, 1988).

The results of the study described here indicated that N-terminal modifications, and to a lesser extent C-terminal modifications, could improve the metabolic stability of Nle[1]-AngIV–derived tri- and tetrapeptides while preserving procognitive and synaptogenic activities. Expanding on these data, additional modifications intended to increase hydrophobicity and decrease hydrogen bonding potential yielded *N*-hexanoic-Tyr-Ile-(6) aminohexanoic amide (dihexa), a potent cognitive-enhancing molecule that proved to be very stable, capable of inducing spinogenesis/synaptogenesis at picomolar concentrations, slowly cleared from the blood compartment, and sufficiently BBB-permeable.

Materials and Methods

Compounds and Peptide Synthesis

Scopolamine hydrobromide (S-1875) was purchased from Sigma-Aldrich (St. Louis, MO). The peptides were synthesized using 9-fluorenylmethoxycarbonyl -based solid-phase peptide synthesis methods and purified by reverse-phase high-pressure liquid chromatography (HPLC) in the Harding laboratory. Purity and structure were verified by liquid chromatography (LC) mass spectrometry (MS).

Serum Metabolism of Peptides

Chemicals and Reagents. HPLC-grade acetonitrile (ACN), acetic acid and water, and reagent-grade trifluoroacetic acid were purchased from Sigma-Aldrich. Nle[1]-AngIV (Nle-Tyr-Ile-His-Pro-Phe), D-Nle-YI, acetyl-NleYIH, γ-amino butyric acid-YIH, NleYI-amide, and N-hexanoic-Tyr-Ile-(6)amino-hexanoic amide (dihexa) were synthesized by 9-fluorenylmethoxycarbonyl-based solid-phase methods in the Harding laboratory.

Animals and Serum Preparation. Four-month-old male Sprague-Dawley rats were used as the blood source for the metabolism studies. Blood was collected from left/right jugular veins of the rats using sterile catheters. After a 30-minute incubation on ice, the blood was centrifuged at 1000 rpm for 15 minutes to separate the serum. Serum was then transferred to clean tubes and stored at −20°C until use.

Drug Solution Preparation. Except for dihexa, all drug solutions were prepared in HPLC-grade water at 5 mg/ml. Stock drugs were kept in powder form and stored at −20°C.

Serum Metabolism Experimental Procedure and Analysis. Rat blood serum samples were pre-equilibrated at 37°C and then 10 μl (50 μg) of each drug solution was added to 90 μl of rat serum in a 1.5-ml Eppendorf tube (Eppendorf North America, Hauppauge, NY) maintained at 37°C. At specified time intervals, metabolism was terminated by precipitating proteins with the addition of 1 ml of a solution of ACN and acetic acid (9:1, v/v). The terminated reaction mixture was stored in a refrigerator (5°C) overnight and centrifuged (14,000 rpm) for 30 minutes to remove precipitated proteins. The separated supernatant was dried in a Savant vacuum concentrator (Thermo Fisher Scientific, Asheville, NC). The dried samples were reconstituted using 200 μl of HPLC mobile phase (10% v/v ACN in water), vortexed briefly, and subjected to HPLC separation and analysis. A serum blank experiment to detect any interfering peaks in the HPLC chromatogram was performed in an identical manner except that no drug was added. Zero time values for each drug candidate were established by first treating the serum with ACN, processing the sample as described previously, adding drug, and then performing HPLC analysis.

The degradation rate of the drugs was determined by measuring the decrease in area under the curve (AUC) at the retention time of the drug over time. The AUC obtained from the zero time experiment was considered to represent the 100% drug concentration and was used to determine the decreased drug concentration at each specified time interval. The semilogarithmic plot of drug concentration versus time was generated to determine the degradation kinetic constant (k) of the tested drug. The half-life of the drug ($t_{1/2}$) was calculated by $0.693/k$.

Apparatus and Chromatographic Conditions. Analysis of samples was performed using a Shimadzu HPLC (Shimadzu, Kyoto, Japan) system. The system consisted of a CBM-20A communications bus module, LC-20AB pumps, and an SPD-M20A photodiode array detector. Data collection and integration were achieved using Shimadzu LC solution software. Separation was achieved using a Rainin Econosphere ODS C18 (250 × 4.6 mm i.d., 5-μm particle size) reverse-phase column obtained from Gilson (Middleton, WI). The column temperature was set at 40°C. The mobile phase consisted of a mixture of ACN and water with 0.1% trifluoroacetic acid and was degassed by ultrasonication. Samples were introduced by manual mode with an injection volume of 250 μl. The drug was eluted with a flow rate of 1 ml/min and detected by photodiode array (PDA) detector at excitation wavelengths of 215 and 280 nm.

IV Pharmacokinetics

Animals and Surgical Procedures. Male Sprague-Dawley rats (≥250 g) were obtained from Harlan Laboratories (Indianapolis, IN) and allowed food (Harlan Teklad rodent diet) and water ad libitum in our animal facility. Ethics approval for animal experimentation was obtained from Washington State University. Rats were housed in temperature-controlled rooms with a 12-hour light/dark cycle. The right jugular veins of the rats were catheterized with sterile polyurethane Hydrocoat catheters (Access Technologies, Skokie, IL) under ketamine (100 mg/kg i.m.; Fort Dodge Animal Health, Fort Dodge, IA) and isoflurane (Vet One, MWI, Meridian, ID) anesthesia. The catheters were exteriorized through the dorsal skin and flushed with heparinized saline before and after blood sample collection and filled with heparin-glycerol locking solution [6 ml glycerol, 3 ml of saline, 0.5 ml of gentamycin (100 mg/ml), 0.5 ml of heparin (10,000 u/ml)] when not sampled for more than 8 hours.

Blood Sample Preparation. Fresh rat blood was obtained before each experiment via jugular vein catheters from adult male Sprague-Dawley rats.

Dihexa solutions were prepared by suspending dry-stock dihexa in dimethyl sulfoxide (DMSO) at 1 mg/ml, and subsequent serial dilutions in 50% DMSO or HPLC-grade water for the final concentrations were specified. Stock dihexa was kept in powder form and stored at −20°C. Quality control samples were prepared by spiking fresh rat plasma with an appropriate dilution of dihexa for the final concentration of dihexa specified, keeping a 10:1 ratio of plasma-to-dihexa solution (final DMSO concentration 5%). The compounds, Nle[1]-AngIV and Nle-YI-(6) aminohexanoic amide, molecules very similar in structure and properties to dihexa, were used as internal standards and were prepared the same way.

The proteins present in the plasma samples were precipitated using three volumes of ice-cold acetonitrile. Internal standards were then added and the samples were vortexed for approximately 10 seconds. Samples were then centrifuged at 5000 rpm for 5 minutes. The supernatants were transferred to new tubes and stored until use at −20°C. Samples were then concentrated in a Savant SpeedVac concentrator to a volume of approximately 100 μl. HPLC-grade water (200 μl) was added to each sample, and the samples were transferred to autosampler vials.

Pharmacokinetic Study. Male Sprague-Dawley rats were catheterized as described in the *Animals and Surgical Procedures* section. Animals were placed in metabolic cages before the start of the study, and time zero blood and urine samples were collected. The animals were then dosed intravenously via the jugular vein catheters or intraperitoneally with dihexa dissolved in 75% DMSO. The typical injection volume was 200 μl, yielding an initial estimated DMSO concentration in blood of 0.46%. After dosing, blood samples were collected as described in Table 1.

After each blood sample was taken, the catheter was flushed with heparinized lactated Ringer's solution, and a volume of heparinized lactated Ringer's solution equal to the volume of blood taken was injected (to maintain total blood volume).

The blood samples were collected into polypropylene microcentrifuge tubes and cooled on ice for not more than 1 hour. The samples were centrifuged at 5000 rpm for 7 minutes, and 80 μl of plasma was transferred into previously prepared tubes containing 240 μl of ice-cold acetonitrile. The samples were vortexed vigorously for 30 seconds and held on ice. Nle-YI-(6) aminohexanoic amide (100 μg/ml) in 10 μl of isotonic saline was used as an internal standard and added to each sample on ice. Samples were held on ice until the end of the experiment and stored at −20°C afterward until further processing.

Serial dilutions of dihexa in 50% DMSO or water (for dilutions of 50 μg/ml or less) were prepared from the stock used to dose the animals to be used for preparation of a standard curve. Ten microliters of each serial dilution was then added to 90 μl of blank plasma for final concentrations of 0.01, 0.02, 0.05, 0.1, 0.2, 1, 10, 20, 50, and 100 μg/ml. Eighty microliters of each plasma sample was transferred to previously prepared tubes containing 240 μl of ice-cold acetonitrile and vortexed vigorously. Ten microliters of isotonic saline containing 100 μg/ml Nle-YI-(6) aminohexanoic amide as an internal standard was added to each sample on ice. The standard-curve plasma samples were then stored at −20°C and further processed alongside the pharmacokinetic study samples according to the method described previously.

Chromatographic System and Conditions. The HPLC/MS system from Shimadzu was used, consisting of a CBM-20A communications bus module, LC-20AD pumps, SIL-20AC auto sampler, SPD-M20A diode array detector, and LCMS-2010EV mass spectrometer. Data collection and integration were achieved using Shimadzu LCMS solution software.

The analytical column that was used was an Econosphere C18 (100 × 2.1 mm) from Grace Davison Discovery Science (Deerfield, IL). The mobile phase consisted of HPLC-grade acetonitrile and water with 0.1% acetic acid. For plasma samples, separation was carried out using a nonisocratic method, starting at 23% ACN and climbing to 31% ACN over 9 minutes, at an ambient temperature and a flow rate of 0.3 ml/min. For MS analysis, a positive ion mode, secondary ion mass spectrometry (SIM) was used to monitor the *m/z* of dihexa at 527 (dihexa with the addition of a sodium adduct) and the *m/z* of Nle-YI-(6) aminohexanoic amide and Nle[1]- AngIV (internal standards) at 513 and 541, respectively (both with sodium adducts). Samples were introduced using the autosampler, and the injection volume was 50 μl. For the microsomal study, the *m/z* of verapamil was 455, the *m/z* of piroxicam was 332, and the *m/z* of 7-ethoxycoumarin was 191.

Pharmacokinetic Analysis. Pharmacokinetic analysis was performed using data from individual rats, from which the mean (S.E.M.) was calculated for each group. Noncompartmental pharmacokinetic parameters were calculated from plasma drug concentration-time profiles by use of WinNonlin software (Pharsight, Mountain View, CA). The following relevant parameters were determined where possible: area under the concentration-time curve from time zero to the last time point ($AUC_{0\text{-last}}$) or extrapolated to infinity ($AUC_{0\text{-}\infty}$), C_{max} concentration in plasma extrapolated to time zero (C_0), terminal elimination half-life ($t_{1/2}$), volume of distribution (V_d), and clearance.

Blood-Brain Barrier Penetrability Study. To evaluate the of ability dihexa to penetrate the BBB and accumulate in the brain, rats were fitted with carotid cannulas and infused with 10 μCi of [^{3}H] dihexa and 2 μCi of [^{14}C]inulin, a vascular space marker, in 100 μl of isotonic saline. Thirty minutes after infusion, brains were removed and dissected and blood samples taken. After solubilization, ^{3}H and ^{14}C were quantified by dual window scintillation counting to determine the amount of dihexa and inulin in brain and blood samples. The dihexa/inulin ratio in the blood was then used to account for any blood contamination in the various brain regions.

Microsomal Metabolism

Male rat liver microsomes were obtained from Celsis (Baltimore, MD). The protocol from Celsis for microsome-drug incubation was followed with minor adaptations. An NADPH-regenerating system (NRS) was prepared as follows: 1.7 mg/ml NADP, 7.8 mg/ml glucose 6-phosphate, and 6 U/ml glucose-6-phosphate dehydrogenase were added to 10 ml 2% sodium bicarbonate. The NRS was used immediately. Five-hundred-micromolar solutions of dihexa, piroxicam, verapamil, and 7-ethoxycoumarin (low, moderate, and highly metabolized controls, respectively) were prepared in acetonitrile. Microsomes were suspended in 0.1 M Tris buffer, pH 7.38, at 0.5 mg/ml. One-hundred-microliter microsomes were added to prechilled microcentrifuge tubes on ice. To each sample, 640 μl of 0.1 M Tris buffer and 10 μl of 500 μM test compound were added. The samples and NRS were placed in a water bath at 37°C for 5 minutes. Samples were removed from the water bath, 250 μl of NRS was added, and each was placed into a rotisserie hybridization oven at 37°C with

TABLE 1
Blood collection schedule following intravenous and intraperitoneal administration of dihexa

Dosage Route	Dose	Blood Sample Volume	Sample Collection Times[a]
	mg/kg	*μl*	
Intravenous	10	200	0, 10, 30, 90, 150, 240, 330, 420, 510, 600, 690, 780, 24 h, 48 h, 5 days
Intraperitoneal	20	200	0, 10, 30, 60, 90, 120, 150, 180, 240, 300, 360, 420, 480, 600, 720, 24 h, 48 h, 5 days

[a] Minutes unless otherwise noted.

rotation at high speed for the appropriate incubation time (10, 20, 30, 40, or 60 minutes). From each sample, 500 μl was transferred to each of two tubes containing 500 μl of ice-cold acetonitrile with internal standard per the incubation sample. Standard curve samples were prepared in an incubation buffer, and 500 μl was added to 500 μl of ice-cold acetonitrile with internal standard. All samples were then analyzed by high-performance liquid chromatography/mass spectrometry. Drug concentrations were determined and loss of parent relative to negative control samples containing no microsomes was calculated. Clearance was determined by nonlinear regression analysis for k_e and $t_{1/2}$ and the equation $Cl_{int} = k_e \times V_d$.

Behavioral Studies

Animals and Surgery. Male Sprague-Dawley rats (Taconic Farms, Germantown, NY) weighing 390 to 450 g were maintained with free access to water and food (Harlan Tekland F6 rodent diet; Harlan, Madison, WI), with the exception of the night before surgery when food was removed, and were used for most studies. The aged rat study used 24-month-old rats of mixed sex. For the scopolamine studies, each animal was anesthetized with ketamine hydrochloride plus xylazine (100 and 2 mg/kg i.m., respectively; Phoenix Scientific, St. Joseph, MO, and Moby, Shawnee, KS). When required, an i.c.v. guide cannula (PE-60; Clay Adams, Parsippany, NY) was stereotaxically positioned (model 900; David Kopf Instruments, Tujunga, CA) in the right hemisphere using flat skull coordinates 1.0 mm posterior and 1.5 mm lateral to the bregma (refer to Wright et al., 1985). The guide cannula measured 2.5 cm in overall length and was prepared with a heat bulge placed 2.5 mm from its beveled tip, thus acting as a stop to control the depth of penetration at 2.5 mm. Once in position, the cannula was secured to the skull with two stainless steel screws and dental cement. The guide was then sealed with a thick stainless steel wire. Postoperatively, the animals were housed individually in an American Accreditation for Laboratory Animal Care–approved vivarium maintained at 22 ± 1°C on a 12-hour alternating light/dark cycle initiated at 6:00 AM. All animals were hand gentled for 5 minutes per day during the 5 to 6 days of postsurgical recovery. Histologic verification of cannula placement was accomplished by the injection of 5 μl of fast-green dye via the guide cannula following the completion of behavioral testing. Correct cannula placement was evident in all rats used in this study.

Water Maze Testing. The water maze consisted of a circular tank painted black (diameter: 1.6 m; height: 0.6 m), filled to a depth of 26 cm with 26–28°C water. A black circular platform (diameter: 12 cm; height: 24 cm) was placed 30 cm from the wall and submerged 2 cm below the water surface. The maze was operationally sectioned into four equal quadrants designated northwest, northeast, southwest, and southeast. For each rat, the location of the platform was randomly assigned to one of the quadrants and remained fixed throughout the duration of training. Entry points were at the quadrant corners (i.e., north, south, east, and west) and were pseudo-randomly assigned such that each trial began at a different entry point than the preceding trial. Three of the four testing room walls were covered with extra-maze spatial cues consisting of different shapes (circles, squares, triangles) and colors. The swimming path of the animals was recorded using a computerized video tracking system (Chromotrack; San Diego Instruments, San Diego, CA). The computer displayed total swim latency and swim distance. Swim speed was determined from these values.

Each member of the treatment groups received an i.c.v. injection of scopolamine hydrobromide [70 nmol in 2 μl of artificial cerebrospinal fluid (aCSF) over a duration of 20 seconds] 20 minutes before testing followed by Nle^1-AngIV or one of the analogs (in 2 μl of aCSF) 5 minutes before testing. Control groups received scopolamine or aCSF 20 minutes before testing followed by aCSF 5 minutes before testing. The behavioral testing protocol has been described previously in detail (Wright et al., 1999). In brief, acquisition trials were conducted on 8 consecutive days with five trials per day. On the first day of training, the animal was placed on the platform for 30 seconds before the first trial. Trials commenced with the placement of the rat facing the wall of the maze at one of the assigned entry points. The rat was allowed a maximum of 120 seconds to locate the platform. Once the animal located the platform, it was permitted a 30-second rest period on the platform. If the rat did not find the platform, the experimenter placed the animal on the platform for the 30-second rest period. The next trial commenced immediately after the rest period.

On the day after acquisition training (day 9), one additional trial was conducted, during which the platform was removed (probe trial). The animal was required to swim the entire 120 seconds to determine the persistence of the learned response. Total time spent within the target quadrant where the platform had been located during acquisition, and the number of crossings of that quadrant was recorded. Upon completion of each daily set of trials, the animal was towel dried and placed under a 100-watt lamp for 10 to 15 minutes and then returned to its home cage.

Dendritic Spine Analysis

Hippocampal Cell Culture Preparation. Hippocampal neurons (2×10^5 cells/cm^2) were cultured from P1 Sprague-Dawley rats on plates coated with poly-L-lysine from Sigma-Aldrich; molecular weight −300,000). Hippocampal neurons were maintained in Neurobasal A media from Invitrogen (Carlsbad, CA) supplemented with B27 from Invitrogen, 0.5 mM L-glutamine, and 5 mM cytosine-D-arabinofuranoside from Sigma-Aldrich added at 2 days in vitro. Hippocampal neurons were then cultured for an additional 3 to 7 days, at which time they were either transfected or treated with various pharmacological reagents as described by Wayman et al. (2008).

Transfection. Neurons were transfected with monomeric red fluorescent protein-β-actin on day 6 in vitro (DIV6) using LipofectAMINE 2000 (Invitrogen) according to the manufacturer's protocol. This protocol yielded the desired 3–5% transfection efficiency, thus enabling the visualization of individual neurons. Higher efficiencies obscured the dendritic arbor of individual neurons. Expression of fluorescently tagged actin allowed clear visualization of dendritic spines, as dendritic spines are enriched in actin. On DIV7, the cells were treated with vehicle (H_20) or peptides (as described in the text) added to media. On DIV12, the neurons were fixed (4% paraformaldehyde, 3% sucrose, 60 mM PIPES, 25 mM HEPES, 5 mM EGTA, 1 mM $MgCl_2$, pH 7.4) for 20 minutes at room temperature and mounted.

Slides were dried for at least 20 hours at 4°C, and fluorescent images were obtained with Slidebook 4.2 Digital Microscopy Software (Olympus America, Inc.; Center Valley, PA) driving an Olympus IX81 inverted confocal microscope (Olympus America) with a 60× oil immersion lens, numerical aperture 1.4, and resolution 0.280 μm. Dendritic spine density was measured on primary and secondary dendrites at a distance of at least 150 μm from the soma. Five 50-μm-long segments of dendrites from at least 10 neurons were analyzed for each data point reported. Each experiment was repeated at least three times using independent culture preparations. Dendrite length was determined using the National Institutes of Health ImageJ 1.41o program (NIH, Bethesda, MD) and the neurite tracing program Neuron J (Meijering et al., 2004). Spines were manually counted.

Organotypic Hippocampal Slice Culture Preparation and Transfection. Hippocampi from P4 Sprague-Dawley rats were cultured as previously described (Wayman et al., 2006). To visualize dendritic arbors, 400-μm hippocampal slices from postnatal day 5 were cultured for 3 days, after which they were biolistically transfected with tomato fluorescent protein using a Helios Gen Gun (BioRad, Hercules, CA), according to the manufacturer's protocol. After a 24-hour recovery period, slices were stimulated with vehicle (H_2O), 1 pM Nle^1-AngIV, or dihexa for 2 days. Slices were fixed and mounted. Hippocampal CA1 neuronal processes were imaged and measured as described above.

Immunocytochemistry. Transfected neurons were treated and fixed as described previously. After fixation, cells were rinsed in

phosphate-buffered saline (PBS) and permeabilized with 0.1% Triton X-100 detergent (Bio-Rad, Hercules, CA), followed by two rinses in PBS and blocked with 8% bovine serum albumin (Intergen Company, Burlington, MA) in PBS for 1 hour. Cells were again rinsed with PBS, followed by a 24-hour incubation period with anti-α-VGLUT1 (Synaptic Systems, Goettingen, Germany), antisynapsin (Synaptic Systems), and antibody to PSD-95 protein (Millipore, Billerica, MA) following the manufacturer's protocol, at 4°C. Subsequently, cells were rinsed twice with PBS, incubated in Alexa Fluor 488 goat-anti-mouse following the manufacturer's protocol (Invitrogen) for 2 hours at room temperature, rinsed again with PBS, and mounted with ProLong Gold antifade reagent (Invitrogen). Imaging and analysis were performed as described previously.

Whole-Cell Recordings. Patch-clamp experiments were performed on mRFP-β-actin–transfected cultured hippocampal neurons with PBS (vehicle control) or 1 pM Nle^1-AngIV pretreatment. Recordings were made on DIV12–DIV14. The culture medium was exchanged by an extracellular solution containing (in mM) 140 NaCl, 2.5 KCl, 1 MgCl2, 3 CaCl2, 25 glucose, and 5 HEPES; pH was adjusted to 7.3 with KOH, and osmolality was adjusted to 310 mOsm. Cultures were allowed to equilibrate in a recording chamber mounted on an inverted microscope (IX-71; Olympus Optical, Tokyo, Japan) for 30 minutes before recording. Transfected cells were visualized with fluorescence (Olympus Optical). Recording pipettes were pulled (P-97 Flaming/Brown micropipette puller; Sutter Instrument, Novato, CA) from standard-wall borosilicate glass without filament (optical density = 1.5 mm; Sutter Instrument). The pipette-to-bath (direct current) DC resistance of patch electrodes ranged from 4.0 to 5.2 MΩ, and were filled with an internal solution of the following composition (in mM): 25 CsCl, 100 CsCH3O3S, 10 phosphocreatine, 0.4 EGTA, 10 HEPES, 2 MgCl2, 0.4 Mg-ATP, and 0.04 Na-GTP; pH was adjusted to 7.2 with CsOH, and osmolality was adjusted to 296-300 mOsm. Miniature postsynaptic excitatory currents (mEPSCs) were isolated pharmacologically by blocking GABA receptor chloride channels with picrotoxin (100 μM; Sigma-Aldrich), blocking glycine receptors with strychnine (1 μM; Sigma-Aldrich), and blocking action potential generation with tetrodotoxin (500 nM; R&D Systems, Minneapolis, MN). Recordings were obtained using a Multiclamp 700B amplifier (Molecular Devices, Sunnyvale, CA). Analog signals were low-pass Bessel filtered at 2 kHz, digitized at 10 kHz through a Digidata 1440A interface (Molecular Devices), and stored in a computer using Clampex 10.2 software (Molecular Devices). The membrane potential was held at −70 mV at room temperature (25°C) during a period of 0.5–2 hours after removal of the culture from the incubator. Liquid junction potentials were not corrected. Data analysis was performed using Clampfit 10.2 software (Molecular Devices) and Mini-Analysis 6.0 software (Synaptosoft Inc.; Fort Lee, NJ). The criteria for a successful recording included an electrical resistance of the seal between the outside surface of the recording pipette and the attached cell >2 GΩ and a neuron input resistance >240 MΩ. The mEPSCs had a 5-minute recording time.

Statistical Analyses

The Morris water maze data sets, consisting of mean latencies and path distances to find the platform during each daily block of five trials, were calculated for each animal for each day of acquisition. One-way analyses of variance (ANOVAs) were used to compare group swim latencies on days 1, 4, and 8 of training. Past experience with this task has indicated these days to be representative of overall performance. Data collected during the probe trials (time spent in the target quadrant and entries into the target quadrant) were also analyzed using one-way ANOVAs. Significant effects were further analyzed by a Newman-Keuls post-hoc test with a level of significance set at $P < 0.05$. Because of variability in the nontreated aged rat group, a nonparametric Mann-Whitney U test was performed to evaluate significance.

One-way ANOVA was used to analyze the dendritic spine results, and significant effects were analyzed by the Tukey post-hoc test. Linear regression analysis was used to determine the correlation between spine characteristics and latency to find the platform in the water maze task. Multiple comparisons of electrophysiological results were made using a one-way ANOVA followed by a Newman-Keuls post-hoc test with a level of significance set at $P < 0.05$. Numerical data are expressed as the mean ± S.E.M.

RESULTS

N- and C-terminal Modifications of Nle^1-AngIV–Derived Peptides Exhibit Improved Stability in Rat Serum

In our quest to develop a BBB-permeable Nle^1-AngIV–-derived molecule with procognitive activity, we have recently determined that the Nle^1-AngIV–derived N-terminal tri- and tetrapeptides possess full biologic activity (Benoist et al., 2011). This observation was critical to reaching our ultimate goal because smaller molecules have a higher probability of breaching the BBB than larger molecules. With this foundation, the next task was to improve the metabolic stability of Nle^1-AngIV–derived N-terminal tri- and tetrapeptides. Previous studies by our laboratory have indicated that angiotensin-like peptides are rapidly metabolized in vivo through the action of aminopeptidases (Dewey et al., 1988). As such, we introduced several structural changes directed at the N-terminal, including the substitution of D-norleucine for L-norleucine, the *N*-acetylation of norleucine, and the replacement of norleucine with the non-α-amino acid γ-aminobutyric acid (GABA) with an expectation of reduced susceptibility to aminopeptidases and overall improved stability. In addition, the impact of converting the C-terminal carboxylic acid to an amide on metabolic stability was also examined.

To evaluate the effect of these structural changes on general metabolic stability, the compounds were incubated in the presence of rat serum and the resultant incubates were analyzed for metabolism by HPLC. The results of this study, which are shown in Table 2, indicate that, as expected, Nle^1-AngIV had an exceedingly short half-life of less than 2 minutes, whereas each of the N-terminal–modified peptides exhibited markedly elongated half-lives. A more modest increase in stability was noted following C-terminal amidation. These data confirm the importance of attenuating N-terminal–dependent degradation, if one desires to improve the metabolic stability of Nle^1-AngIV–derived peptides. Thus, the incorporation of these types of modifications or the introduction of nonpeptide bonds (Krebs et al., 1996) may provide a workable strategy to improve the bioavailability of Nle^1-AngIV–derived peptides and peptidomimetics.

TABLE 2
Serum stability of AngIV analogs
Values are the mean ± S.D. (N = 3).

Compound	Half-Life
	min
Nle^1-AngIV	1.42 ± 0.26
N-Acetyl-Nle-Tyr-Ile-His	115 ± 7.6
D-Nle-Tyr-Ile	225 ± 23.7
GABA-Tyr-Ile	946 ± 234
Nle-Tyr-Ile-His-NH_2	23.0 ± 3.1
Dihexa	335.5 ± 9.5

N- and C-terminal–Modified Nle^1-AngIV Analogs Retain Procognitive Activity

Although N-terminal–modification of Nle^1-AngIV–derived tri- and tetrapeptides significantly increased their stability in rat serum, the true test of success of these structural modifications is whether the molecules still possess procognitive activity. To gauge the procognitive potential of the molecules, we evaluated their capacity to reverse scopolamine-dependent learning deficits following their acute i.c.v. application as assessed by performance in the Morris water maze. The scopolamine preparation that was employed is a widely accepted animal model of the spatial memory dysfunction and produces deficits reminiscent of those observed in early to middle-stage Alzheimer's disease patients (Fisher et al., 2003).

As an initial measure of cognitive function, the escape latency to locate the submerged pedestal in a Morris water maze was recorded over an 8-day observation period. As can be seen in Fig. 1A, scopolamine application significantly retarded task acquisition when compared with vehicle controls. Tandem application of scopolamine with each of the N- and C-terminal–modified peptides significantly improved water maze performance when compared with the scopolamine-treated group. Although there were no differences among the groups on day 1 of training, all of the compound-treated groups showed improved performance by day 3 ($P < 0.001$). This improved performance was maintained throughout the testing period, and post-hoc analyses on day 8 confirmed that all had improved performance when compared with the scopolamine/deficit group ($P < 0.0001$). On day 8, animals treated with GABA-Tyr-Ile exhibited the best performance among the compound-treated groups; had a significantly lower mean latency to find the platform than the other three treated groups ($P < 0.001$), which did not differ from one another ($P > 0.05$); and were not significantly different than the vehicle control group ($P > 0.05$).

As a second measure of cognitive function, the persistence and strength of the learned task was assessed with a probe trial on day 9 (Fig. 1B). The rats were exposed to the maze with no pedestal for 2 minutes, and time spent in the quadrant that originally contained the submerged pedestal was determined. These data mirrored the escape latency results, with all treated groups performing better than the scopolamine/deficit group ($P < 0.01$–0.001). Again, the performance by the group treated with GABA-Tyr was superior to all other compound-treated groups ($P < 0.05$–0.01) and not different from the vehicle control group ($P > 0.05$).

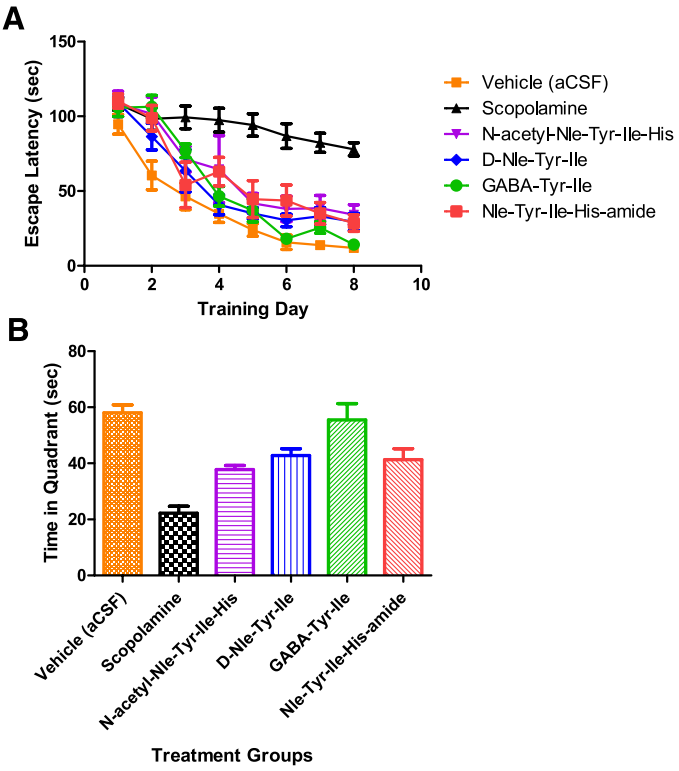

Fig. 1. Metabolically stabilized AngIV analogs reverse scopolamine-dependent spatial learning deficits. (A) group latencies to find the submerged platform in the Morris water maze task of spatial memory. Data from six groups of rats ($N = 8$ each) that were pretreated with scopolamine (70 nmol i.c.v. in 2 μl of aCSF) 20 minutes before training followed by the infusion of the designated analog (1 nmol i.c.v. in 2 μl of aCSF) 5 minutes before daily training are shown. A two-way ANOVA with repeated measures indicated that all groups were different from the scopolamine→aCSF on at the last 5 days of testing. Mean ± SEM; $P < 0.001$. (B) day 9 probe trials by each experimental group. Time spent in the target quadrant was recorded for each experimental group. All treatment groups were different from the scopolamine→aCSF group ($P < 0.01$) but not significantly different from the vehicle group ($P > 0.05$). The GABA-Tyr-Ile group was also different from all of the other treated groups ($P < 0.05$).

N- and C-terminal–Modified Nle^1-AngIV Analogs Stimulate Dendritic Spinogenesis

As part of our recent evaluation of C-terminal–truncated fragments of Nle^1-AngIV, we demonstrated that Nle^1-AngIV and only its cognitively active C-terminal–truncated fragments were effective stimulators of dendritic spinogenesis on cultured hippocampal neurons from neonatal rats. As such, the expectation was that the cognitively active fragments described in this study would also support hippocampal spinogenesis. As can be seen from the dose-response curves presented in Supplemental Fig. 1, A–D, this expectation was borne out for each of the metabolically stabilized molecules. The only surprise from this study was that GABA-Tyr-Ile, which had consistently exhibited the most profound procognitive activity, did not appear to be the most potent generator of new dendritic spines.

Dihexa Is a Metabolically Stabilized, Blood-Brain Barrier–Permeable Molecule

The data presented in Table 2 indicate that increased stability can be imparted to Nle^1-AngIV–derived compounds by both N- and C-terminal modification. In addition, the functional studies summarized in Fig. 1 indicate that replacement of norleucine in the number 1 position with the straight-chain, non-α-amino acid GABA yielded a molecule with superior procognitive activity. With this information in hand, we synthesized a series of compounds, exemplified by dihexa, that not only were protected at both terminals, but also contained the replacement of norleucine with a straight-chain acyl group. Instead of simply appending a non-α-amino, long, straight-chain amino acid to the N-terminal, we chose to eliminate the N-terminal amine entirely, which increased overall hydrophobicity and removed a critical hydrogen bonding site. As can be seen in Table 2, these modifications significantly increased the serum stability of dihexa in comparison with Nle^1-AngIV.

The purpose of elongating the N-terminal acyl group and removing the N-terminal amino group was to increase the probability that resultant molecules might be BBB-permeable and access the brain parenchyma. To evaluate the success of the modifications that were incorporated in dihexa in this regard, rats were fitted with carotid cannulas and infused with 10 μCi of [^{3}H]dihexa and 2 μCi of [^{14}C]inulin, a vascular space marker. Thirty minutes after infusion, brains were removed and dissected and blood samples were taken. After solubilization, ^{3}H and ^{14}C were quantified by dual window scintillation counting to determine the amount of dihexa and inulin in brain and blood samples. The ratio of dihexa/inulin in the blood was then used to account for any blood contamination in the various brain regions. More importantly, ^{3}H/^{14}C ratios above that observed in the blood were indicative of dihexa being concentrated. As can be seen in Fig. 2, all of the brain regions examined avidly concentrated dihexa, attesting to its ability to cross the BBB.

Dihexa Has a Long Circulating Half-Life

To begin to evaluate the potential clinical utility of dihexa, adult male Sprague-Dawley rats were administered 10 mg/kg dihexa intravenously and in-vivo pharmacokinetics were determined. An example of the resulting plasma concentration/time profile is shown in Supplemental Fig. 2. Dihexa exhibited rapidly decreasing plasma levels from 0 to 4 hours, suggesting that both distribution and elimination occurred during this period. After 4 hours, the rate of clearance declined and plasma levels became more stable, exhibiting a relatively linear rate of decline, suggesting a phase of pure elimination from 4 to 120 hours. The exception from the linearly declining pattern of plasma levels was between 8.5 to 13 hours, when plasma levels were actually lower than at 24 hours. These results suggest that a small fraction of dihexa undergoes enterohepatic recirculation, which could cause an increase in plasma levels. Elevations in plasma concentration due to enterohepatic recirculation are usually observed after a meal when bile containing drug is released into the duodenum and the drug is reabsorbed from the intestine. Since rats were allowed food 12 hours after the onset of the study, any enterohepatic recirculation would be expected to occur subsequent to 12 hours, the time period that corresponded with rising plasma levels of dihexa.

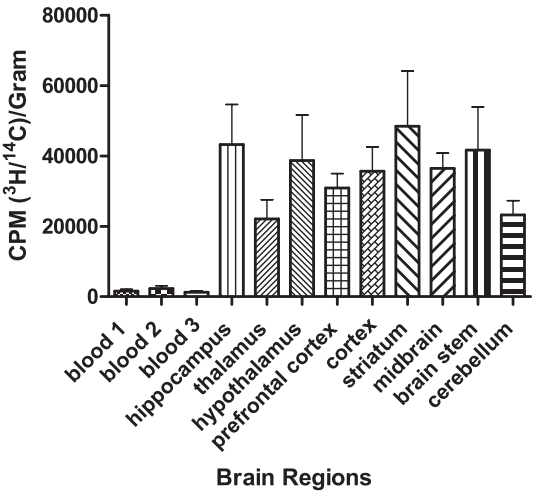

Fig. 2. Dihexa is concentrated in multiple brain regions. Rats fitted with a carotid cannula were anesthetized and infused with 0.5 ml of isotonic saline containing 10 μCi of [^{3}H]dihexa and 2 μCi of [^{14}C]inulin, a vascular marker. Thirty minutes after infusion, the rats were decapitated, the brains were removed, and various brain regions were dissected. The tissues were then weighed and solubilized with NCS tissue solubilizer, an organic protein solubilizing agent, and 10 ml of scintillation was added. Samples were counted with a scintillation counter using two different windows to quantitate both ^{3}H and ^{14}C counts. ^{3}H /^{14}C ratios were determined so that blood-derived dihexa contamination of tissues could be determined. The results indicate that all brain regions concentrated dihexa ($P < 0.001$) compared with blood, but no area was statistically different from any other ($P > 0.05$). The average ^{3}H /^{14}C ratio for blood was 1687 (mean ± S.E.M.; $n = 4$). Counts Per Minute (CPM), XXXX.

Relevant pharmacokinetic parameters for dihexa as determined after i.v. dosing are summarized in Table 3. Plasma data were modeled by noncompartmental analysis using WinNonlin software. Dihexa exhibited a long half-life ($t_{1/2}$) of 12.68 days following i.v. administration and similarly when delivered intraperitoneally [8.83 ± 2.41 days (mean ± S.E.M.); $N = 4$). Dihexa appeared to be extensively distributed outside the central blood compartment and/or bound within the tissues as evidenced by its large V_d. These results, which suggest that dihexa is very hydrophobic (logP), are in agreement with the outcome of Quantitative structure–activity relationship (QSAR) modeling estimates generated by the ADMET Predictor (Simulations Plus, Inc.; Lancaster, CA) that calculated an octanol/water partition coefficient of 177.8 for dihexa (Table 4).

Not surprisingly because of its stability, hydrophobic character, and small size, dihexa was predicted to be orally bioavailable. The predicted effective human jejunal permeability (P_{eff}) value represents the predicted effective human jejunal permeability of the molecule (Table 4). The predicted P_{eff} value for dihexa (1.78) is intermediate between the predicted P_{eff} values for enalapril (1.25) and piroxicam (2.14), two orally bioavailable drugs. Dihexa was also predicted to be 22.59% unbound to plasma proteins in circulation, thus making it available for distribution into the tissues.

In addition to contributing to its slow removal from the blood was a lack of phase I metabolism. Phase I metabolism of dihexa, which was determined using pooled male rat liver microsomes, was found to be very low, with an average intrinsic clearance (Cl_{int}) of 2.72 μl/min/mg and an average half-life of 509.4 minutes. To provide a context for dihexa's clearance rate, the stability of piroxicam (60.2 μl/min/mg), verapamil (112.5 μl/min/mg), and 7-ethoxycoumarin (136.7 μl/min/mg) was also monitored as high-, moderate-, and low-metabolized standards, respectively. The clearance rates previously indicated were within the published ranges for these often-employed standards (Di et al., 2004; Shou et al., 2005; Lu et al., 2006; Behera et al., 2008). The clearance time courses for dihexa and the standards fit curves defining single-phase exponential decay processes with R^2 values between of 0.96 and 0.99 (Supplemental Fig. 3).

TABLE 3
Dihexa pharmacological parameters ($N = 3$)

Pharmacokinetic Parameter	Mean ± S.E.M.
$AUC_{0-\infty}$ (min/μg/ml)	4471 ± 1408
V_d (l/kg)	54.4 ± 14.8
C_p^0 (μg/ml)	87.3 ± 31.9
$t_{1/2}$ (min)	18,256 ± 7787
KE (min^{-1})	0.00007 ± 0.00004
CL (l/min/kg)	0.0026 ± 0.0007

CL, clearance; C_p^0, plasma concentration at time zero; KE, elimination half-life.

TABLE 4
Predicted physicochemical properties of dihexa

Physicochemical Property	Predicted Value
LogP	2.25
P_{eff}	1.78
P_{avg}	0.62
Pr_{Unbnd}	22.59

P_{avg}, predicted average intestinal permeability along the entire human intestinal tract; Pr_{Unbnd}, percent of drug not bound to plasma proteins.

Dihexa Exhibits Procognitive Activity

The essential test of the success of the structural modifications incorporated into dihexa was whether it possessed procognitive activity like its parent compound Nle[1]- AngIV. Therefore, dihexa's ability to reverse scopolamine-dependent deficits in the water maze performance was established. The initial study, which was simply tasked with verifying the procognitive activity of dihexa, entailed the direct brain delivery of dihexa via an i.c.v. cannula. The data presented in Fig. 3A confirm our expectation that dihexa would retain biologic activity. Both the low- and high-dose groups of dihexa yielded significantly improved performance when compared with the scopolamine group from day 2 of testing on ($P < 0.001$). The high-dose group was indistinguishable from the vehicle control group at all testing days ($P > 0.05$).

Since the ultimate goal of the project was to produce a clinically relevant molecule that could be delivered peripherally but still exhibit procognitive/antidementia activity, the effectiveness of both the intraperitoneal and oral delivery routes of dihexa administration were determined using the scopolamine model. As can be seen in Fig. 3, B and C, both delivery methods yielded the anticipated biologic activity. Furthermore, both studies indicated a clear dose-response relationship between the dose of dihexa and water maze performance. The high doses of each method of delivery (i.p. = 0.5 mg/kg per day; oral = 2.0 mg/kg per day) produced performances that were significantly improved over that seen in the scopolamine groups ($P < 0.001$) and indistinguishable from vehicle controls ($P > 0.05$).

Probe trials on day 9 were again used to evaluate the strength and persistence of the learned task. As can been seen in Fig. 4, A, B, and C, dihexa at its highest dose significantly ($P < 0.001$) increased the time spent in the target quadrant compared with the scopolamine-impaired groups, regardless of the delivery method used and was not different from nonscopolamine-treated controls ($P > 0.05$). In each case where multiple doses of dihexa were used, the probe trial data yielded a dose-response relationship similar to that observed for escape latencies.

Although the scopolamine model is often used to assess the cognitive-enhancing capacity of experimental molecules, it clearly initiates learning deficits in a nonphysiological manner that only results in acute deficits. To begin to assess the clinical potential of dihexa as an antidementia drug, we chose to evaluate its effects on a more physiological-relevant model: the aged Sprague-Dawley rat. Rats, similar to humans, develop age-related cognitive difficulties. Typically, ~50% of rats exhibit impaired performance in the water maze compared with 3-month-old rats (Zeng et al., 2012). As such, we evaluated the ability of orally delivered dihexa (2 mg/kg per day) to impact water maze learning in 24-month-old Sprague-Dawley rats of mixed sex. As expected, the results shown in Fig. 5 indicate that

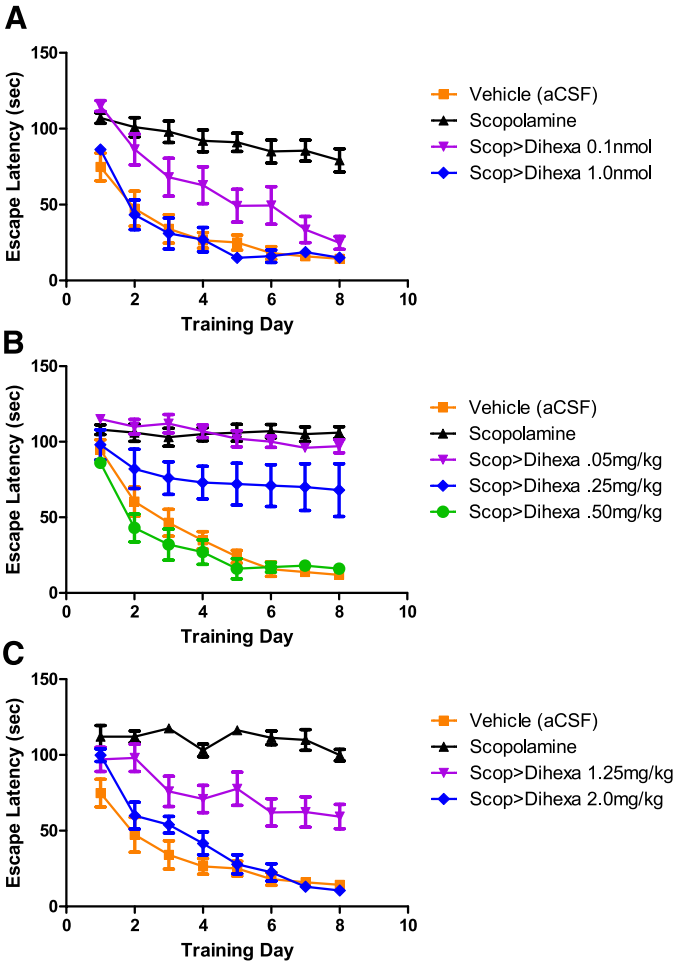

Fig. 3. Dihexa reverses scopolamine-dependent spatial learning deficits. Group latencies to find the submerged platform in the Morris water maze task of spatial memory are shown. Twenty minutes before beginning testing, 3-month-old male Sprague-Dawley rats received scopolamine directly into the brain (i.c.v.), and 15 minutes later dihexa was given either i.c.v., i.p., or orally. There were 5 trials per day for 8 days. The latency to find the pedestal was considered a measure of learning and memory. (A) rats were pretreated with scopolamine (scop) (70 nmol i.c.v. in 2 μl of aCSF) 20 minutes before training followed by the i.c.v. infusion of dihexa (0.1 or 1 nmol in 2 μl of aCSF) 5 minutes before daily training. A two-way ANOVA with repeated measures indicated that all time points for the 1-nmol dihexa group were different from the scopolamine group, which received vehicle (aCSF) instead of dihexa ($P < 0.001$). The lower, 0.1 nmol, dose of dihexa also significantly improved performance when compared with the scopolamine group on days 5–8 of testing ($P < 0.05$). (B) rats were pretreated with scopolamine (70 nmol i.c.v. in 2 μl of aCSF) 20 minutes before training followed 15 minutes later by an i.p. injection of dihexa in DMSO (<1%) at 0.05, 0.25, or 0.50 mg/kg. A two-way ANOVA with repeated measures indicated that the latency curves for dihexa at 0.25 and 0.50 mg/kg were different from the scopolamine→aCSF group's learning curve ($P < 0.001$). The 0.50 mg/kg group was not different from the vehicle control group ($P > 0.05$), and the 0.05 mg/kg dihexa group was not different from the scopolamine group ($P > 0.05$). (C) rats were pretreated with scopolamine (70 nmol i.c.v. in 2 μl of aCSF) 20 minutes before training followed by oral delivery (gavage) of dihexa at 1.25/kg and 2.0 mg/kg (suspension in isotonic NaCl) 5 minutes before daily training. The high oral dose (2 mg/kg) of dihexa completely reversed the scopolamine-dependent learning deficit (***$P < 0.001$), whereas the effect of scopolamine was partially reversed at the 1.25 kg/mg dose on days 3–8 ($P < 0.01$). Mean ± S.E.M.; n = 8–10.

dihexa significantly improved performance ($P < 0.05$) on most of the test days. It should be noted that because these aged rats were not prescreened for cognitive deficits, the results substantially underestimate the effect of dihexa. The expectation

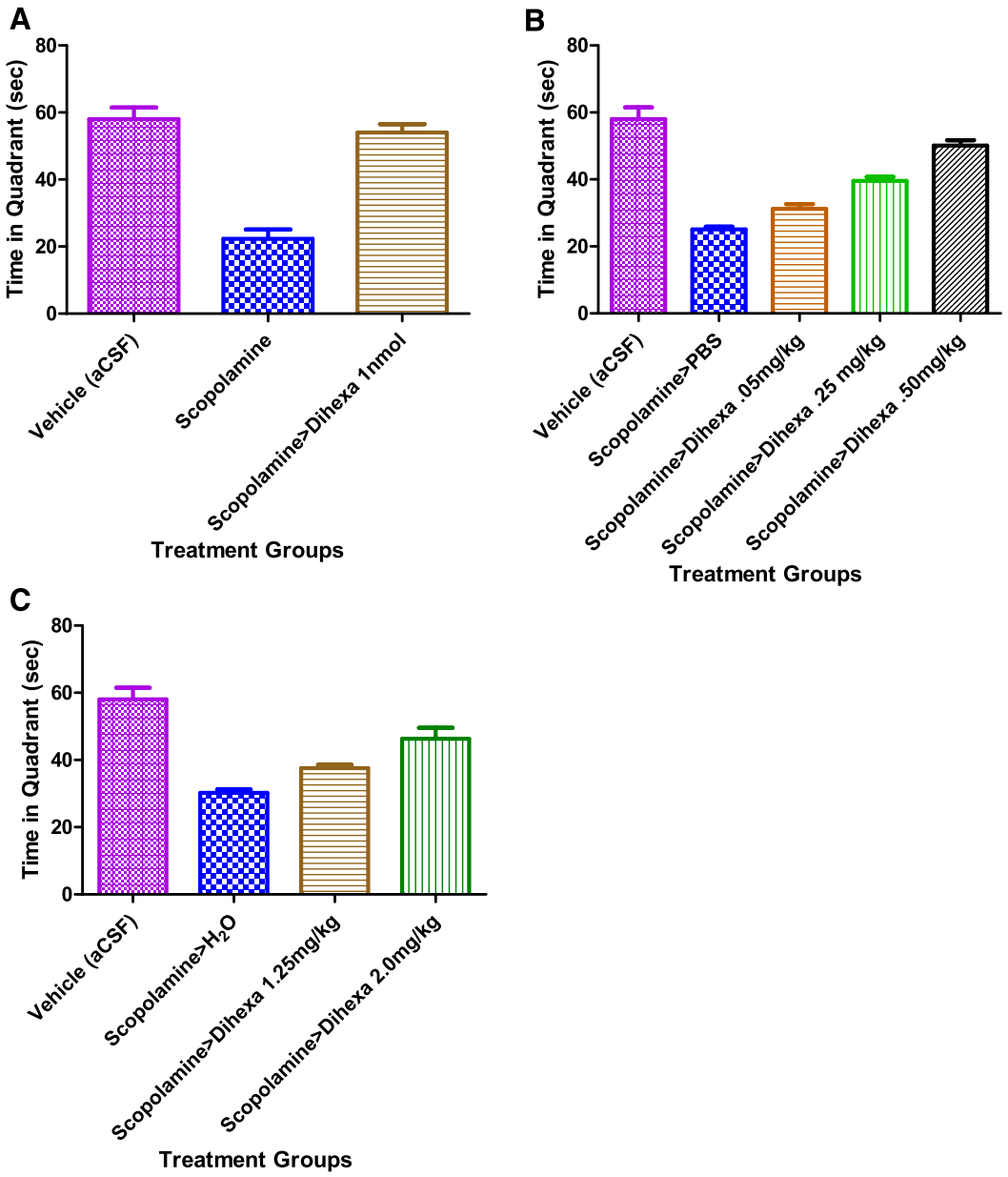

Fig. 4. Dihexa increases time in the target quadrant during day 9 probe trials. Time spent in the target quadrant was recorded for each experimental group following i.c.v., i.p., and oral delivery of dihexa. (A) in the i.c.v. study, the scopolamine group performed below the chance level (30 s) and was significantly different from the vehicle control group and the scopolamine→dihexa 1-nmol group ($P < 0.001$), whereas the scopolamine→dihexa 1-nmol and vehicle control groups were not different ($P > 0.05$). (B) in the i.p. delivery study, the scopolamine→PBS group performed below the chance level and was different from the vehicle control group ($P < 0.001$). Each of the treatment groups was different from the scopolamine→PBS group ($P < 0.001$–$P < 0.05$), whereas each of the treatment groups was different from one another ($P < 0.001$–$P < 0.05$), exhibiting the same dose-response relationship observed in the initial water maze study (Fig. 3). (C) in the oral delivery study, the scopolamine→H_2O group performed near the chance level and was different from the vehicle control group ($P < 0.001$). Both of the treatment groups were different than the scopolamine→H_2O group ($P < 0.05$ and $P < 0.001$, respectively), whereas both of the treatment groups were different from one another ($P < 0.001$), exhibiting the same dose-response relationship observed in the initial water maze study (Fig. 3). Mean ± S.E.M.; n = 8–10.

that only half of the untreated rats would be effective learners even without dihexa treatment likely contributed to the high variability in escape latencies seen with the untreated group.

Dihexa Induces Spinogenesis in Cultured Hippocampal Neurons

Recently, the procognitive effects of Nle^1-AngIV, the parent compound of dihexa, and several C-terminal–truncated analogs have been correlated with their ability to induce dendritic spine formation and the establishment of new synapses (Benoist et al., 2011). As such, the influence of dihexa on spinogenesis and synaptogenesis in high-density mRFP-β-actin–transfected rat hippocampal neuronal cultures was evaluated. Actin-enriched spines increased in number in response to both dihexa (Fig. 6, B and D) and Nle^1-AngIV (Fig. 6, C and D) following 5 days of treatment at 10^{-12} M concentration that started on the seventh day in vitro (DIV7). The results revealed a near 3-fold increase in the number of spines stimulated by dihexa and a greater than

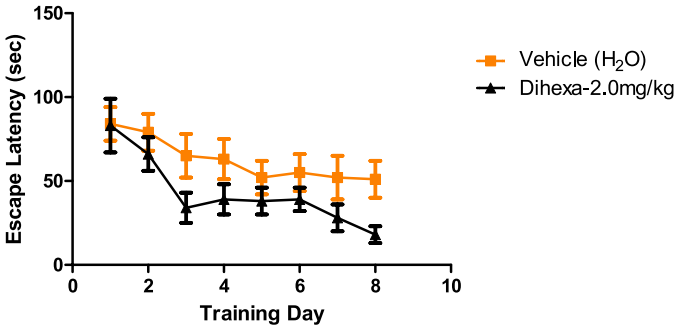

Fig. 5. Dihexa improves spatial learning in aged rats. Group latencies to find the submerged platform in the Morris water maze task of spatial memory are shown. Five minutes before beginning testing, 24-month-old mixed sex (3 male and 3 female per group) Sprague-Dawley rats were administered dihexa (2 mg/kg) orally by gavage (suspension in isotonic NaCl) on a daily basis. There were five trials per day for 8 days. The latency to find the pedestal was considered a measure of learning and memory. The learning curve for the treated rats was significantly different from that of the nontreated rats (Mann-Whitney U test, $P < 0.03$). Mean ± S.E.M.; $n = 6$.

2-fold increase for Nle^1-AngIV. Both treatment groups differed significantly from the vehicle control group for which the average number of spines per 50-μm dendrite length was 15. The average number of spines for the dihexa- and Nle^1-AngIV–treated groups was 41 and 32 spines per 50-μm dendrite length, respectively (mean ± S.E.M., $n = 200$ dendritic segments; $P < 0.001$ by one-way ANOVA and Tukey post-hoc test).

The i.c.v. water maze data with dihexa indicate a modest but significant improvement in spatial learning performance even on the first day of testing, thus suggesting that the underlying mechanism responsible for the behavior must be rapidly engaged. Therefore, the ability of both dihexa and Nle^1-AngIV to promote spinogenesis was assessed following an acute 30-minute application on the final day of culturing (Fig. 6E). The acute 30-minute application of dihexa and Nle^1-AngIV, on the 12th day in vitro (DIV12), reveals a significant increase in spines compared with 30-minute vehicle-treated neurons (dihexa mean spine numbers per 50-μm dendrite length = 23.9; Nle^1-AngIV mean spine numbers per 50-μm dendrite length = 22.6; vehicle control–treated neurons mean spine numbers per 50-μm dendrite length = 17.4; $n = 60$; $P < 0.0001$ by one-way ANOVA followed by Tukey post-hoc test).

Strong correlations exist between spine size, persistence of spines, number of AMPA-receptors, and synaptic efficacy. A correlation between the existence of long-term memories to spine-head volume has also been suggested (Kasai et al., 2010; Yuste and Bonhoeffer, 2001; Yasumatsu et al., 2008). With these considerations in mind, spine-head size measurements were taken following 5 days of drug treatment. Results indicate that the 10^{-12} M dose of dihexa and Nle^1-AngIV both increased spine-head width (Supplemental Fig. 4). The mean spine-head width for Nle^1-AngIV was 0.87 μm, 0.80 μm for dihexa, and 0.67 μm for vehicle controls.

Dihexa and Nle^1-AngIV Mediate Synaptogenesis

To begin to assess the functionality of the newly formed dendritic spines, mRFP-β-actin–transfected neurons were immunostained for three synaptic markers. Hippocampal neurons were stimulated for 5 days in vitro with 10^{-12} M dihexa or Nle^1-AngIV (Fig. 7). Since glutamate synaptic transmission is known to involve receptors that reside on dendritic spines, neurons were probed for excitatory synaptic transmission by staining for the glutamatergic presynaptic marker vesicular glutamate transporter 1 (VGLUT1) (Balschun et al., 2010). The universal presynaptic marker synapsin was also visualized to assess the juxtaposition of the newly formed spines with presynaptic boutons (Ferreira and Rapoport, 2002). Finally, PSD-95 served as a marker for the postsynaptic density (El Husseini et al., 2000).

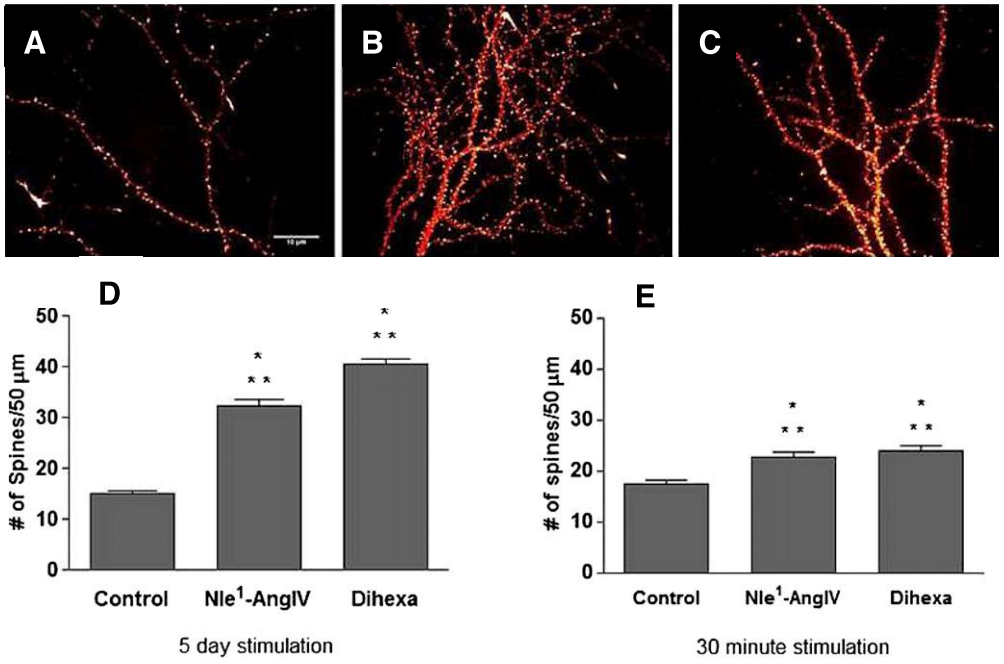

Fig. 6. Nle^1-AngIV and dihexa increase the number of dendritic spines. Time-dependent effects of Nle^1-AngIV- and dihexa-treated neurons on spinogenesis are presented. Hippocampal neurons transfected with mRFP-β-actin were treated with 10^{-12} M dihexa or 10^{-12} M Nle^1-Ang IV for 5 days or 30 minutes in culture before fixation on DIV12. (A) representative image of the dendritic arbor of a 5-day vehicle-treated hippocampal neuron. (B) representative image of a dendritic arbor from a neuron stimulated for 5 days with 10^{-12} M dihexa. (C) representative image of the dendritic arbor of a neuron stimulated with 10^{-12} M Nle^1-Ang IV for 5 days. (D) bar graph representing the number of spines per 50-μm dendrite length per treatment condition following a 5-day in vitro treatment. ***$P < 0.001$; $n = 200$ dendritic segments. (E) bar graph representing the number of spines per 50-μm dendrite length per treatment condition after an acute 30-minute treatment. ***$P < 0.001$; $n = 60$ dendritic segments. Mean ± S.E.M. Analysis by one-way ANOVA and Tukey's post-hoc test.

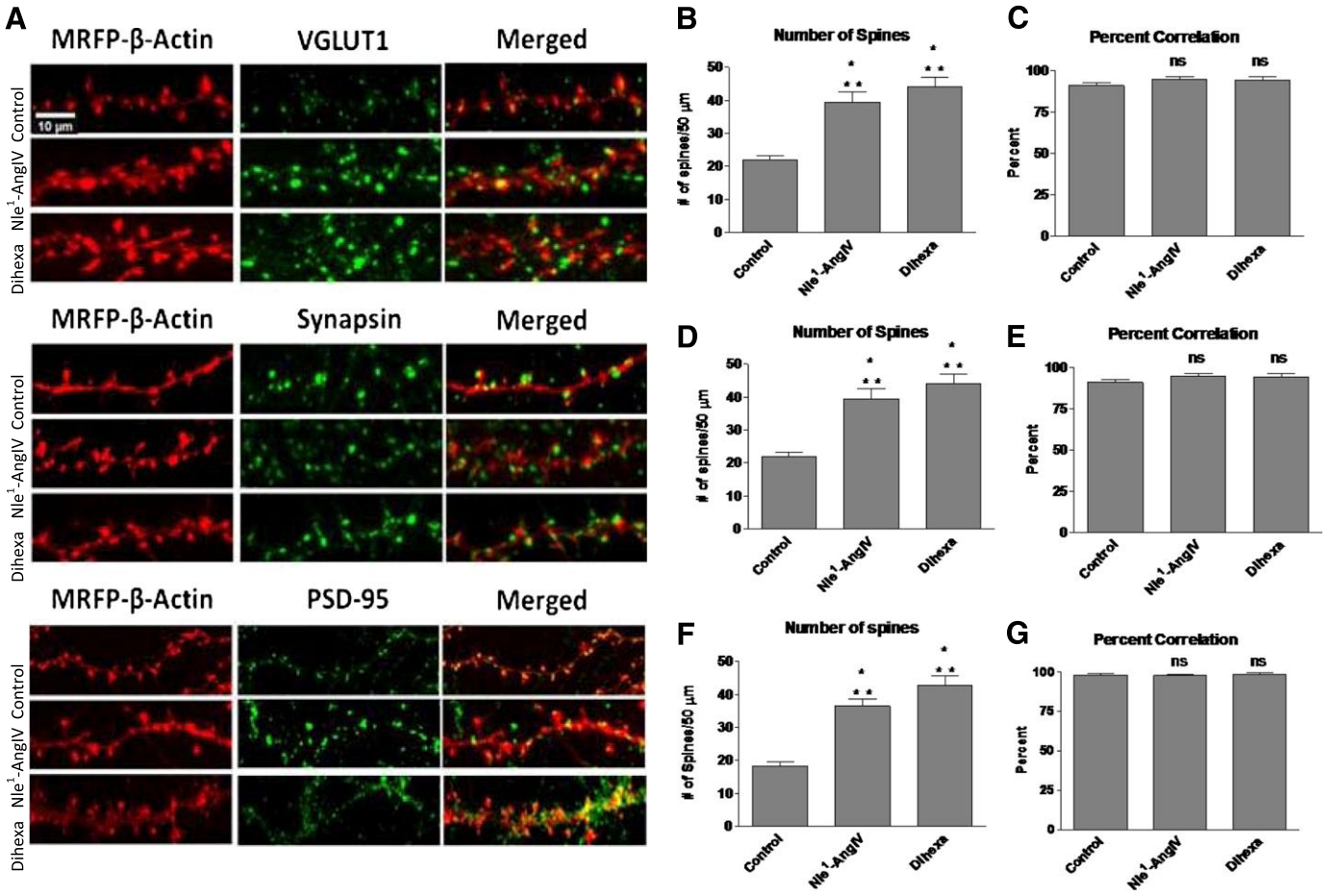

Fig. 7. Localization of synaptic markers following Nle[1]-AngIV and dihexa-dependent dendritic spine induction. Dihexa- and Nle[1]-AngIV-treated neurons were immunostained for the universal presynaptic marker synapsin, the glutamatergic presynaptic marker VGLUT1, and the postsynaptic density maker PSD-95. The percent correlation between the postsynaptic spines (red) and presynaptic puncta (green), which represented a different marker in each panel, was determined and used as an indicator of functional synapses. (A) representative images of hippocampal neurons transfected with mRFP-β-actin and immunostained for the excitatory presynaptic marker VGLUT1, the general presynaptic marker synapsin, and the postsynaptic marker PSD-95 following a 5-day treatment with vehicle, 10^{-12} M Nle[1]-AngIV, or 10^{-12} M dihexa. (B) bar graph confirming the expected increase in the number of dendritic spines following treatment with vehicle, Nle[1]-AngIV, or dihexa (***$P < 0.001$; mean ± S.E.M.; $n = 25$ dendritic segments). (C) bar graph showing the percent correlation between dendritic spines after treatment and the glutamatergic presynaptic marker VGLUT1. No significant differences between the stimulated neurons and vehicle control–treated neurons were observed ($P > 0.05$; mean ± S.E.M.; $n = 25$ dendritic segments). (D) bar graph confirming the expected increase in the number of dendritic spines following treatment with vehicle, Nle[1]-AngIV, or dihexa (***$P < 0.001$; mean ± S.E.M.; $n = 25$ dendritic segments). (E) bar graph showing the percent correlation between dendritic spines after treatment and the general presynaptic marker synapsin. No significant differences between the stimulated neurons and vehicle control–treated neurons were observed ($P > 0.05$; mean ± S.E.M.; $n = 25$ dendritic segments). (F) bar graph confirming the expected increase in the number of dendritic spines following treatment with vehicle, Nle[1]-AngIV, or dihexa (***$P < 0.001$; mean ± S.E.M.; $n = 25$ dendritic segments). (G) bar graph showing the percent correlation between dendritic spines after treatment and the postsynaptic marker PSD-95. No significant differences between the stimulated neurons and vehicle control–treated neurons were observed ($P > 0.05$; mean ± S.E.M.; $n = 25$ dendritic segments). Together, these data indicate that dendritic spines formed after treatment support functional synapses. ns, not significant.

Again, dihexa and Nle[1]-AngIV treatment significantly augmented dendritic spinogenesis (Fig. 7, B, D, and F) in each of the three studies [mean spine numbers for the combined studies for Nle[1]-AngIV = 39.4, for dihexa = 44.2 and for vehicle-treated neurons = 23.1 (mean ± S.E.M., $P < 0.001$)]. The percent correlation for the newly formed spines with synaptic markers VGLUT1, synapsin, or PSD-95 is shown in Fig. 7, D, and E. Dihexa and Nle[1]-AngIV treatment-induced spines did not differ from control-treated neurons in the percent correlation to VGLUT1, synapsin, or PSD-95 ($P > 0.05$), indicating that the newly formed spines contained the same synaptic machinery as already-present spines. The previous results suggest that the newly formed dendritic spines produced by dihexa and Nle[1]-AngIV treatment create functional synapses.

To further support this conclusion, mEPSCs, the frequency of which corresponds to the number of functional synapses, were recorded from mRFP-β-actin–transfected hippocampal neurons (Fig. 8). The mean frequency of AMPA-mediated mEPSCs recorded from vehicle-treated neurons was 3.06 ± 0.23 Hz from 33 cells, while Nle[1]-AngIV induced a 1.7-fold increase [5.27 ± 0.43 Hz from 25 cells (mean ± S.E.M.); $P < 0.001$ versus control group] and dihexa produced a 1.6-fold increase (4.82 ± 0.34 Hz from 29 cells; $P < 0.001$ versus control group), confirming the expected expansion of functional synapses. No differences in amplitude, rise, or decay times were observed (data not shown), which suggests that the individual properties of the synapse were not altered.

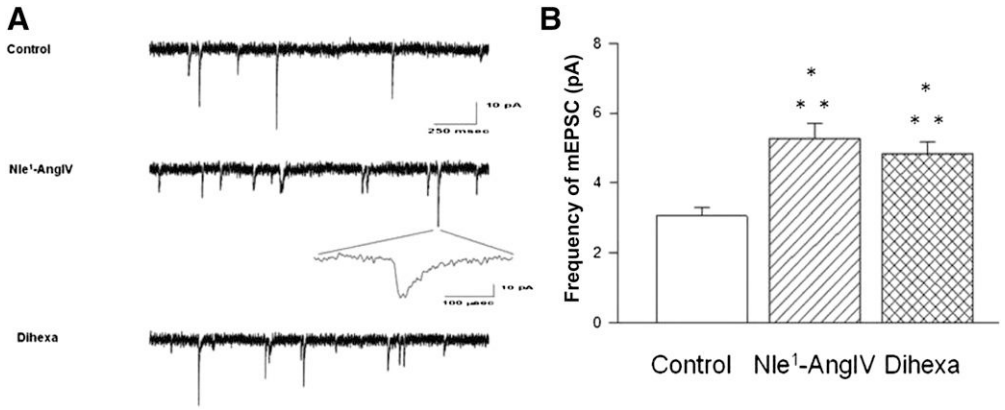

Fig. 8. Increased frequencies of mEPSCs in dissociated hippocampal neurons treated with Nle[1]-AngIV and dihexa. Recordings were carried out on rat dissociated hippocampal neurons treated with vehicle, 10^{-12} M Nle[1]-AngIV, or 10^{-12} M dihexa for 5 days before recording. The postsynaptic currents, which were recorded in the presence of strychnine, picrotoxin, and tetrodotoxin, represented spontaneous bursts likely mediated by AMPA receptors. (A) representative traces of mEPSC recordings from Nle[1]-AngIV- or dihexa-treated hippocampal neurons. (B) bar graph illustrating the increase in mEPSC frequencies in hippocampal neurons that resulted from Nle[1]-AngIV or dihexa treatment. The increased frequencies indicate that dendritic spines induced by Nle[1]-AngIV or dihexa support functional synaptic transmission. $^{***}P < 0.001$; mean ± S.E.M.; $n = 25$.

Dihexa and Nle[1]-AngIV Induce Spinogenesis in Hippocampal Organotypic Cultures

To further assess the physiologic significance of the spine induction witnessed in dissociated neonatal hippocampal neurons, the effects of dihexa and Nle[1]-AngIV on spine formation in organotypic hippocampal slice cultures were evaluated. These preparations, while still neonatal in origin, represent a more intact and three-dimensional environment than dissociated neurons. Hippocampal CA1 neurons, which have been functionally linked to hippocampal plasticity and learning/memory, were easily identified based on morphologic characteristics and were singled out for analysis. Dihexa and Nle[1]-AngIV significantly augmented spinogenesis in organotypic hippocampal slice cultures when compared with vehicle-treated neurons. There were no differences in spine numbers between the dihexa and Nle[1]-AngIV treatment groups (Supplemental Fig. 5). Spine numbers measured for control slices were 7 per 50-μm dendrite length versus 11 spines per 50-μm dendrite length for both Nle[1]-AngIV- and dihexa-treated neurons (mean ± S.E.M., n = 13–20 dendritic segments; $P < 0.01$).

DISCUSSION

The goal of this study was to develop an AngIV-derived molecule that retained the procognitive/antidementia activity of AngIV and Nle[1]-AngIV but possessed improved pharmacokinetic properties, thus allowing it to penetrate the BBB in sufficient quantities to reach therapeutic levels in the brain. The culmination of this effort was dihexa, a hydrophobic, N- and C-terminal–modified, AngIV-related peptide. The cursory pharmacokinetic characterization of dihexa included in this study indicated that it was stable in serum, had a long circulating half-life, and penetrated the BBB. Data from behavioral studies using scopolamine amnesia and aged rat models, where dihexa was able to reverse cognitive deficits, indicated that the metabolic stability and BBB permeability of dihexa were apparently high enough to attain therapeutic brain levels after oral administration. Additional mechanistic studies demonstrated that both dihexa and Nle[1]-AngIV, its parent compound, were effective stimulators of hippocampal synaptogenesis, thus providing a rational explanation for their procognitive activities.

The starting point for this study was a recently published study (Benoist et al., 2011) that determined that the information in Nle[1]-AngIV critical to its procognitive activity resided in its three to four N-terminal amino acids. Using the N-terminal tripeptide of Nle[1]-AngIV as a starting point, the intermediate goal of this study was to establish the impact of various N- and C-terminal modifications of peptide stability. The results indicated that N-terminal modifications were particularly effective at enhancing metabolic stability, whereas C-terminal amidation offered more modest protection. The observation that replacement of the N-terminal norleucine with GABA yielded a compound with superior antidementia activity indicated that an N-terminal α-amino group was not required for activity. Furthermore, these data suggested that N-terminal, *N*-acyl tyrosine containing tripeptides should be biologically active. This observation, coupled with the added stability contributed by C-terminal amidation and the desire to increase the hydrophobicity of the peptide, led to the generation of a series of compounds with the structure *N*-acyl-Tyr-Ile-(6) amino-hexanoic amide. After preliminary functional screening (see the following paragraphs), *N*-hexanoic-Tyr-Ile-(6) amino-hexanoic amide was chosen for further investigation with the expectation that it would be biologically active, metabolically stable, and BBB-permeable.

Although not the focus of this study, an obvious question relates to the identity of the molecular target responsible for the procognitive and synaptogenic activity of dihexa and other AngIV-related compounds. Hints to the answer to this question can be found in four recent articles (Yamamoto et al., 2010; Kawas et al., 2011, 2012; Wright et al., 2012), which clearly demonstrate that both the peripheral and central nervous system actions of AT_4 receptor antagonists depend on their ability to inhibit the hepatocyte growth factor (HGF)/c-Met (HGF receptor) system by binding to and blocking HGF activation. Conversely, we (C. C. Benoist, Kawas LH, and Harding, JW, unpublished data) have recently demonstrated that both Nle[1]-AngIV and dihexa bind HGF, leading to its activation, and that the procognitive and/

or synaptogenic actions of these compounds are blocked by both HGF and c-Met antagonists. With this knowledge in hand, a library of *N*-acyl-Tyr-Ile-(6) amino-hexanoic amide analogs was screened for their capacity to potentiate the biologic activity of HGF. This screen identified the hexanoic N-terminal substituent as the most active compound.

The ultimate goal of this project was to produce a clinically useful pharmaceutical for the treatment of dementia, including Alzheimer's disease. At its core, dementia results from a combination of diminished synaptic connectivity among neurons and neuronal death in the entorhinal cortex, hippocampus, and neocortex. Therefore, an effective treatment would be expected to augment synaptic connectivity, protect neurons from underlying death inducers, and stimulate the replacement of lost neurons from pre-existing pools of neural stem cells. These clinical endpoints advocate for the therapeutic use of neurotrophic factors, which mediate neural development, neurogenesis, neuroprotection, and synaptogenesis. Not unexpectedly, neurotrophic factors have been considered as treatment options for many neurodegenerative diseases, including Alzheimer's disease (see reviews: Calissano et al., 2010; Nagahara and Tuszynski, 2011). The realization that activation of the HGF/c-Met system represents a viable treatment option for dementia should be no surprise. HGF is a potent neurotrophic factor in many brain regions (Ebens et al., 1996; Kato et al., 2009), while affecting a variety of neuronal cell types. However, the direct use of HGF or any other protein neurotrophic factor as a therapeutic agent has two serious limitations: 1) large size and hydrophilic character, which preclude BBB permeability; and 2) the need to be manufactured by recombinant methods at high cost, thus limiting its widespread use. The development of dihexa has seemingly overcome these impediments by virtue of its oral activity, demonstrated procognitive/antidementia activity, and anticipated low manufacturing costs. Among planned future studies, designed to gauge the clinical potential of dihexa, will be a direct comparison of dihexa to several approved antidementia therapeutics using rodent dementia models.

Authorship Contributions

Participated in research design: McCoy, Benoist, Wright, Harding, Appleyard, Wayman, Kawas.

Conducted experiments: McCoy, Benoist, Zhu, Kawas, Bule-Ghogare, Wright.

Contributed new reagents or analytic tools: Harding.

Performed data analysis: McCoy, Harding, Benoist, Kawas, Wright, Bule-Ghogare, Zhu.

Wrote or contributed to the writing of the manuscript: McCoy, Benoist, Wright, Kawas, Bule-Ghogare, Appleyard, Wayman, Harding.

REFERENCES

Abhold RH and Harding JW (1988) Metabolism of angiotensins II and III by membrane-bound peptidases from rat brain. *J Pharmacol Exp Ther* **245**:171–177.

Balschun D, Moechars D, Callaerts-Vegh Z, Vermaercke B, Van Acker N, Andries L, and D'Hooge R (2010) Vesicular glutamate transporter VGLUT1 has a role in hippocampal long-term potentiation and spatial reversal learning. *Cereb Cortex* **20**: 684–693.

Behera D, Damre A, Varghese A, and Addepalli V (2008) In vitro evaluation of hepatic and extra-hepatic metabolism of coumarins using rat subcellular fractions: correlation of in vitro clearance with in vivo data. *Drug Metabol Drug Interact* **23**: 329–350.

Benoist CC, Wright JW, Zhu M, Appleyard SM, Wayman GA, and Harding JW (2011) Facilitation of hippocampal synaptogenesis and spatial memory by C-terminal truncated Nle1-angiotensin IV analogs. *J Pharmacol Exp Ther* **339**:35–44.

Braszko JJ, Kupryszewski G, Witczuk B, and Wiśniewski K (1988) Angiotensin II-(3-8)-hexapeptide affects motor activity, performance of passive avoidance and a conditioned avoidance response in rats. *Neuroscience* **27**:777–783.

Calissano P, Matrone C, and Amadoro G (2010) Nerve growth factor as a paradigm of neurotrophins related to Alzheimer's disease. *Dev Neurobiol* **70**:372–383.

De Bundel D, Smolders I, Vanderheyden P, and Michotte Y (2008) Ang II and Ang IV: unraveling the mechanism of action on synaptic plasticity, memory, and epilepsy. *CNS Neurosci Ther* **14**:315–339.

Dewey AL, Wright JW, Hanesworth JM, and Harding JW (1988) Effects of aminopeptidase inhibition on the half-lives of [125I]angiotensins in the cerebroventricles of the rat. *Brain Res* **448**:369–372.

Di L, Kerns EH, Gao N, Li SQ, Huang Y, Bourassa JL, and Huryn DM (2004) Experimental design on single-time-point high-throughput microsomal stability assay. *J Pharm Sci* **93**:1537–1544.

Ebens A, Brose K, Leonardo ED, Hanson MG, Jr, Bladt F, Birchmeier C, Barres BA, and Tessier-Lavigne M (1996) Hepatocyte growth factor/scatter factor is an axonal chemoattractant and a neurotrophic factor for spinal motor neurons. *Neuron* **17**: 1157–1172.

El-Husseini AE, Schnell E, Chetkovich DM, Nicoll RA, and Bredt DS (2000) PSD-95 involvement in maturation of excitatory synapses. *Science* **290**:1364–1368.

Faure S, Chapot R, Tallet D, Javellaud J, Achard JM, and Oudart N (2006) Cerebroprotective effect of angiotensin IV in experimental ischemic stroke in the rat mediated by AT(4) receptors. *J Physiol Pharmacol* **57**:329–342.

Ferreira A and Rapoport M (2002) The synapsins: beyond the regulation of neurotransmitter release. *Cell Mol Life Sci* **59**:589–595.

Fisher A, Pittel Z, Haring R, Bar-Ner N, Kliger-Spatz M, Natan N, Egozi I, Sonego H, Marcovitch I, and Brandeis R (2003) M1 muscarinic agonists can modulate some of the hallmarks in Alzheimer's disease: implications in future therapy. *J Mol Neurosci* **20**:349–356.

Gard PR (2004) Angiotensin as a target for the treatment of Alzheimer's disease, anxiety and depression. *Expert Opin Ther Targets* **8**:7–14.

Gard PR (2008) Cognitive-enhancing effects of angiotensin IV. *BMC Neurosci* **9** (Suppl 2):S15.

Kasai H, Fukuda M, Watanabe S, Hayashi-Takagi A, and Noguchi J (2010) Structural dynamics of dendritic spines in memory and cognition. *Trends Neurosci* **33**: 121–129.

Kato N, Nakanishi K, and Nemoto K (2009) Efficacy of HGF gene transfer for various nervous injuries and disorders. *Cent Nerv Syst Agents Med Chem* **9**:300–306.

Kawas LH, McCoy AT, Yamamoto BJ, Wright JW, and Harding JW (2012) Development of angiotensin IV analogs as hepatocyte growth factor/Met modifiers. *J Pharmacol Exp Ther* **340**:539–548.

Kawas LH, Yamamoto BJ, Wright JW, and Harding JW (2011) Mimics of the dimerization domain of hepatocyte growth factor exhibit anti-Met and anticancer activity. *J Pharmacol Exp Ther* **339**:509–518.

Kramár EA, Armstrong DL, Ikeda S, Wayner MJ, Harding JW, and Wright JW (2001) The effects of angiotensin IV analogs on long-term potentiation within the CA1 region of the hippocampus in vitro. *Brain Res* **897**:114–121.

Kramár EA, Harding JW, and Wright JW (1997) Angiotensin II- and IV-induced changes in cerebral blood flow. Roles of AT1, AT2, and AT4 receptor subtypes. *Regul Pept* **68**:131–138.

Krebs LT, Kramár EA, Hanesworth JM, Sardinia MF, Ball AE, Wright JW, and Harding JW (1996) Characterization of the binding properties and physiological action of divalinal-angiotensin IV, a putative AT4 receptor antagonist. *Regul Pept* **67**:123–130.

Lee J, Albiston AL, Allen AM, Mendelsohn FA, Ping SE, Barrett GL, Murphy M, Morris MJ, McDowall SG, and Chai SY (2004) Effect of I.C.V. injection of AT4 receptor ligands, NLE1-angiotensin IV and LVV-hemorphin 7, on spatial learning in rats. *Neuroscience* **124**:341–349.

Lu C, Li P, Gallegos R, Uttamsingh V, Xia CQ, Miwa GT, Balani SK, and Gan LS (2006) Comparison of intrinsic clearance in liver microsomes and hepatocytes from rats and humans: evaluation of free fraction and uptake in hepatocytes. *Drug Metab Dispos* **34**:1600–1605.

Meijering E, Jacob M, Sarria JC, Steiner P, Hirling H, and Unser M (2004) Design and validation of a tool for neurite tracing and analysis in fluorescence microscopy images. *Cytometry A* **58**:167–176.

Mustafa T, Lee JH, Chai SY, Albiston AL, McDowall SG, and Mendelsohn FA (2001) Bioactive angiotensin peptides: focus on angiotensin IV. *J Renin Angiotensin Aldosterone Syst* **2**:205–210.

Nagahara AH and Tuszynski MH (2011) Potential therapeutic uses of BDNF in neurological and psychiatric disorders. *Nat Rev Drug Discov* **10**:209–219.

Pederson ES, Krishnan R, Harding JW, and Wright JW (2001) A role for the angiotensin AT4 receptor subtype in overcoming scopolamine-induced spatial memory deficits. *Regul Pept* **102**:147–156.

Shou WZ, Magis L, Li AC, Naidong W, and Bryant MS (2005) A novel approach to perform metabolite screening during the quantitative LC-MS/MS analyses of in vitro metabolic stability samples using a hybrid triple-quadrupole linear ion trap mass spectrometer. *J Mass Spectrom* **40**:1347–1356.

Stubley-Weatherly L, Harding JW, and Wright JW (1996) Effects of discrete kainic acid-induced hippocampal lesions on spatial and contextual learning and memory in rats. *Brain Res* **716**:29–38.

von Bohlen und Halbach O (2003) Angiotensin IV in the central nervous system. *Cell Tissue Res* **311**:1–9.

Wayman GA, Davare M, Ando H, Fortin D, Varlamova O, Cheng H-YM, Marks D, Obrietan K, Soderling TR, and Goodman RH, et al. (2008) An activity-regulated microRNA controls dendritic plasticity by down-regulating p250GAP. *Proc Natl Acad Sci USA* **105**:9093–9098.

Wayman GA, Impey S, Marks D, Saneyoshi T, Grant WF, Derkach V, and Soderling TR (2006) Activity-dependent dendritic arborization mediated by CaM-kinase I activation and enhanced CREB-dependent transcription of Wnt-2. *Neuron* **50**:897–909.

Wright JW, Clemens JA, Panetta JA, Smalstig EB, Weatherly LA, Kramár EA, Pederson ES, Mungall BH, and Harding JW (1996) Effects of LY231617 and angiotensin IV on ischemia-induced deficits in circular water maze and passive avoidance performance in rats. *Brain Res* **717**:1–11.

Wright JW and Harding JW (2010) The brain RAS and Alzheimer's disease. *Exp Neurol* **223**:326–333.
Wright JW, Morseth SL, Abhold RH, and Harding JW (1985) Pressor action and dipsogenicity induced by angiotensin II and III in rats. *Am J Physiol* **249**: R514–R521.
Wright JW, Stubley L, Pederson ES, Kramár EA, Hanesworth JM, and Harding JW (1999) Contributions of the brain angiotensin IV-AT4 receptor subtype system to spatial learning. *J Neurosci* **19**:3952–3961.
Wright JW, Wilson WL, Wakeling V, Boydstun AS, Jensen A, Kawas LH, and Harding JW (2012) The angiotensin IV analogue and hepatocyte growth factor/c-Met antagonist, divalinal-AngIV, attenuates the acquisition of methamphetamine-dependent condition place preference in rats. *Brain Sci* **2**: 298–318.
Yamamoto BJ, Elias PD, Masino JA, Hudson BD, McCoy AT, Anderson ZJ, Varnum MD, Sardinia MF, Wright JW, and Harding JW (2010) The angiotensin IV analog Nle-Tyr-Leu-psi-(CH2-NH2)3-4-His-Pro-Phe (norleual) can act as a hepatocyte growth factor/c-Met inhibitor. *J Pharmacol Exp Ther* **333**:161–173.
Yasumatsu N, Matsuzaki M, Miyazaki T, Noguchi J, and Kasai H (2008) Principles of long-term dynamics of dendritic spines. *J Neurosci* **28**:13592–13608.
Yuste R and Bonhoeffer T (2001) Morphological changes in dendritic spines associated with long-term synaptic plasticity. *Annu Rev Neurosci* **24**:1071–1089.
Zeng Y, Lv F, Li L, Yu H, Dong M, and Fu Q (2012) 7,8-dihydroxyflavone rescues spatial memory and synaptic plasticity in cognitively impaired aged rats. *J Neurochem.* **122**:800-11.

Address correspondence to: Dr. Joseph W. Harding, Department of Veterinary and Comparative Anatomy, Pharmacology, and Physiology, P.O. Box 6520, Washington State University, Pullman, WA 99164-6520. E-mail: hardingj@vetmed.wsu.edu